Structure, morphology, and magnetic properties of high-performance NiCuZn ferrite*

He Xue-Min(何学敏), Yan Shi-Ming(颜士明), Li Zhi-Wen(李志文), Zhang Xing(张 星), Song Xue-Yin(宋雪银), Qiao Wen(乔 文), Zhong Wei(钟 伟)†, and Du You-Wei(都有为)

Collaborative Innovation Center of Advanced Microstructures, National Laboratory of Solid State Microstructures, Jiangsu Provincial Laboratory for NanoTechnology and Department of Physics, Nanjing University, Nanjing 210093, *China*

(Received 5 April 2015; revised manuscript received 5 August 2015; published online 20 October 2015)

High-performance submicron-scaled NiCuZn ferrites are prepared by the solid-state reaction method through using CuO as additive. In the synthesis process, a mixture of superfine powder is sintered at 900 °C for 3 h, and the obtained product is NiZn-ferrite with spinel structure. We observe that the particle size increases with raising the sintering temperature. The NiCuZn ferrite with relatively uniform size and granular shape has the best performance: its coercivity is 14 Oe (1 Oe = 79.5775 A·m^{-1}) and saturation magnetization is 48 emu/g. We also study the effects of particle size, magnetocrystalline anisotropy, and microstructure on coercivity. The method presented here is convenient and economical for producing the high-permeability ferrite powders.

Keywords: soft-magnetic properties, size effect, magnetocrystalline anisotropy

PACS: 75.20.En, 75.30.Gw, 75.50.Gg **DOI:** 10.1088/1674-1056/24/12/127502

1. Introduction

With the advance in assembling technology, electronic equipment develops towards the microminiaturization and multi-species, electronic devices also have more bright prospects. Recently, the soft magnetic ferrites have been utilized widely and commercialized rapidly. Based on the soft ferrite materials, the electronic devices gradually develop into a chip, multilayer, and multifunction type.[1] As a kind of soft magnetic ferrite, spinel NiZn ferrite exhibits high electrical resistivity (10^6 Ω·cm), high permeability in radio frequency (RF) region, and little eddy current loss in a 10–500 MHz range;[2–4] therefore, it has applications at high frequencies, e.g., serving as antenna rods, suppression of electromagnetic interference, broad-band transformers, loading coils, microwave devices, anti-EMI circuits, etc.[5–10]

As is well known, the properties of ferrite materials are strongly influenced by composition and microstructures, which are sensitive to the preparation methodology used in their synthesis process.[11] In addition, the sintering conditions employed and the impurity levels present in or added to these materials also change their properties.[12] To obtain high relative initial permeability, NiZn ferrite needs a coarse and compact microstructure;[13] thus the sintering temperature usually must be higher than 1100 °C.[14–16] However, the high sintering temperature brings about a series of problems, including high losses, higher power consumption, etc.[17–19] Even worse, this sintering temperature is still too high to co-fire with Ag conductor which possesses a melting temperature of 961 °C. Obviously, developing a suitable process to fabricate high-performance NiZn ferrites and modifying the composition to reduce the sintering temperature below 900 °C are necessary.

It has been shown that adding CuO to NiZn ferrite could lower its sintering temperature with a conventional solid-state reaction method.[20–23] At the same time, the addition of appropriate Cu^{2+} can effectively enhance the density and electrical resistivity of ferrites, and improve the electromagnetic properties. Actually, the obtained products are NiCuZn ferrites, and they have been extensively applied in various inductance devices, e.g. multilayer chip inductor (MLCI), LC combination element, chip magnetic bead, filter, etc.[24–27] Furthermore, cobalt as an important member of the additive family is widely used in the actual production of soft-magnetic ferrites due to the large positive magnetocrystalline anisotropy of Co ferrite.[28–30] On the one hand, small additions of Co^{3+} can compensate for negative magnetocrystalline anisotropy K_1 of host ferrites, and thus enhance the initial permeability of NiZn ferrites.[31] On the other hand, the cobalt-induced uniaxial anisotropy is conducive to improving the cut-off frequency, reducing the hysteresis loss, and improving the temperature characteristic.[32] It is thus held that the low-temperature synthesis of high-performance NiCuZn ferrites can be achieved by using appropriate CuO and a little cobalt.

Therefore, in the present article we are to add both CuO

*Project supported by the National Natural Science Foundation of China (Grant Nos. 11174132, 11474151, and U1232210), the National Key Project for Basic Research, China (Grant Nos. 2011CB922102 and 2012CB932304), the Innovation Program for Doctoral Research of Jiangsu Province, China (Grant No. CXZZ13_0035), and the Priority Academic Program Development of Jiangsu Provincial Higher Education Institutions, China.

†Corresponding author. E-mail: wzhong@nju.edu.cn

© 2015 Chinese Physical Society and IOP Publishing Ltd

and Co_3O_4 for preparing high-performance NiCuZn ferrites at low sintering temperatures. The microstructures and magnetic properties of ferrite powder can be well controlled by regulating the sintering temperature in a range of 750 °C–1000 °C. The effects of particle size D, lattice parameter a, morphology, and magnetocrystalline anisotropy on the magnetic properties (magnetization M and coercivity H_C) are analyzed. Finally, we demonstrate that the NiCuZn-ferrite powder (0.19 μm in average size) exhibiting excellent magnetic properties can be obtained through 900 °C calcination.

2. Experiment

The chemical reagent-grade powders of Fe_2O_3, NiO, CuO, ZnO, and Co_3O_4 were chosen as the raw materials to prepare NiCuZn ferrites. According to the formula of $Ni_{0.276}Cu_{0.113}Zn_{0.604}Co_{0.008}Fe_{1.81}O_4$, all oxides were mixed with distilled water and stirred in a ball mill, thereby giving a reddish-brown slurry. Under ambient conditions, the slurry was milled for 18 h using a planetary mill, and then was dried at 100 °C for 12 h. After drying, the superfine powder was kept inside a lid-covered alumina crucible and was heated in a furnace to a selected temperature in a range of 750 °C–1000 °C (heating rate = 10 °C/min) and maintained at that temperature for 3 h. At the end, the reaction mixture was cooled down to room temperature, and the obtained powder was ground. As shown in Table 1, we obtained six samples (M1–M6) by adopting six different sintering temperatures (750, 800, 850, 900, 950, and 1000 °C).

Table 1. Values of lattice parameter (a), particle size (D), coercivity (H_C), remanent magnetization (M_r), and saturation magnetization (M_s) of the NiCuZn-ferrite powder samples obtained after sintering at different values of temperature (T).

Sample	T/°C	a/Å	D/μm	H_C/Oe	M_r/(emu/g)	M_s/(emu/g)
M1	750	8.455(4)	0.14	38.89	1.12	15.17
M2	800	8.437(4)	0.15	32.08	1.53	22.10
M3	850	8.435(5)	0.16	25.17	2.22	33.73
M4	900	8.431(8)	0.19	14.16	2.54	48.19
M5	950	8.430(3)	0.29	10.11	1.93	52.14
M6	1000	8.427(9)	0.34	6.82	1.45	57.74

The x-ray diffraction (XRD) patterns were examined in the 2θ range from 10° to 90° with an X'TRA powder diffractometer using the Cu Kα radiation. For the analysis of XRD data, the particle size D was deduced from the width of XRD maxima by applying the classical Scherrer formula, and the lattice parameter a was refined with the Rietveld method using the GSAS program. Scanning electron microscopy (SEM) images were obtained over an FEI Sirion200 field-emission instrument operated at an acceleration voltage of 5 kV. Based on the Nano Measurer software, the size distribution was recorded by manually measuring the equivalent diameter of >100 particles from the corresponding SEM images. Room-temperature hysteresis loops were measured using a Lake Shore 7304 vibrating sample magnetometer (VSM) in an applied magnetic field of 6 kOe. Accordingly, the coercivity H_C, remanent magnetization M_r, and saturation magnetization M_s were analyzed in detail.

3. Results and discussion

The sintering temperature of the mixed powders will influence the crystallization, particle size, and shape of the obtained samples. Figure 1 shows the XRD patterns of the NiCuZn ferrites which are sintered at various temperatures. We can see that the crystal structures of all the samples are the same as that of spinel NiZn ferrite. For all of them, the strongest peak located at $2\theta = 35.408°$ is ascribable to (311) diffraction, and these sharp diffraction peaks indicate that the NiCuZn ferrite is well crystalline above the sintering temperature of $\geqq 750$ °C. Moreover, the sharpening of the XRD peak with the increase of sintering temperature is ascribed to grain growth as well as to the reduction of internal stress.

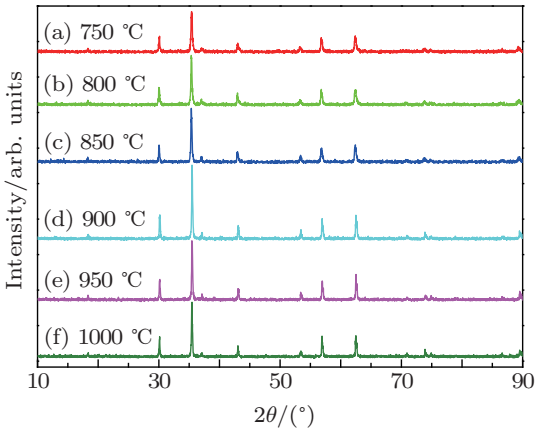


Fig. 1. (color online) XRD patterns of NiCuZn-ferrite powder samples generated after sintering at different temperatures for 3 h.

To study the influence of lattice parameter a on the magnetic properties of NiCuZn-ferrite powder, we conduct Rietveld analysis of the XRD patterns based on the $NiZnFe_2O_4$ phase of cubic (Fd-3m) structure, and the refinement results are shown in Fig. 2. It can be seen that XRD refinement has very high accuracy, thereby giving a reasonable lattice parameter.

As shown in Table 1 and Fig. 3, these a values are larger than that of $NiZnFe_2O_4$ (JCPDS No. 08-0234, a = 8.399 Å).[33] With the increase of sintering temperature, there is monotonic decline of a value. With the rise of crystallization temperature, the phenomenon of lattice thermal expansion and small grain boundary happen in ferrite, so as to reduce the lattice parameter a. Also, the partial Ni^{2+} is replaced by Zn^{2+} and Cu^{2+}, thereby giving a smaller a value.[34,35] In addition,

the diminution of lattice parameter indicates that the heat treatment is very effective for enhancing the grain compactness. Actually, the change of lattice parameter reflects a process like this: firstly, metal oxides are gradually decomposed to form oxygen and metal ions when the as-milled superfine powder reaches a certain temperature; then O^{2-} constitutes tetrahedral (A) and octahedral (B) sites, while Fe^{2+}, Zn^{2+}, Ni^{2+}, Cu^{2+}, Fe^{3+} cations are distributed between A and B sites; finally, the obtained spinel structure becomes better with increasing sintering temperature.

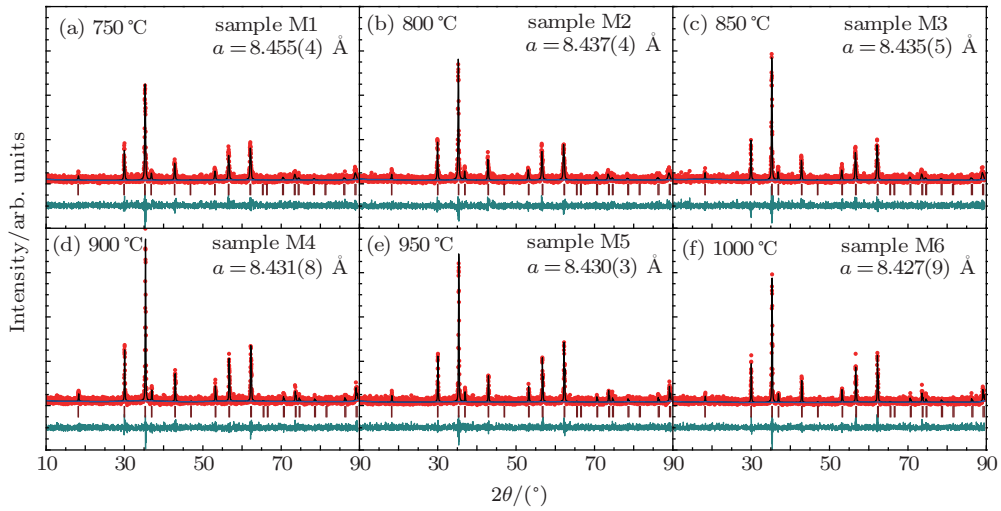


Fig. 2. (color online) Results of XRD Rietveld analysis for the NiCuZn-ferrite powder samples M1–M6. Shown at the top right corner is the calculated lattice parameter a.

According to the Scherrer formula,[36] the relationship of particle size D and the full width at half maximum (FWHM), β, of a diffraction peak can be expressed as

$$D = 0.89\lambda/\beta\cos\theta, \tag{1}$$

where λ is the wavelength of incident x-ray, and θ denotes the Bragg diffraction angle. Actually, the broadening β is simply caused by the grain refinement and expressed as $\beta = (\beta_M^2 - \beta_S^2)^{1/2}$,[37] where β_M is the practically measured FWHM, and β_S denotes the broadening of apparatus itself. To eliminate the instrumental broadening of the setup, β_S can be obtained by adopting the FWHM of the measured bulk crystal. As evaluated based on Eq. (1), the average sizes of the NiCuZn-ferrite powder samples M1–M6 are 0.14, 0.15, 0.16, 0.19, 0.29, and 0.34 μm, respectively. It is noted that the particle size of NiCuZn-ferrite powder increases with increasing sintering temperature as shown in Table 1 and Fig. 3. As can be seen from Fig. 3, the change of a is not obvious when the sintering temperature is above 900 °C, but the particle size increases significantly. Since the sintering temperature at 900 °C is a turning point, it is envisaged that the morphologies and magnetic properties of M5 and M6 are significantly different from those of M1–M3.

Figure 4 shows the typical SEM images of the M1–M6 samples, and the corresponding size distributions are shown in Fig. 5. Overall, the change of morphology with sintering temperature is rather distinct. With sintering temperature increasing from 750 °C to 850 °C (see Figs. 4(a)–4(c)), the obtained powders have granular appearance, while the average particle size and size distribution present certain changes. As shown in Figs. 5(a)–5(c), the average sizes are 0.141, 0.153, and 0.162 μm for the M1–M3 samples sintered at 750, 800, and 850 °C, respectively. At a sintering temperature of 900 °C, the obtained NiCuZn ferrites become uniform particles in appearance (Fig. 4(d)). As can be seen from Fig. 5(d), the particles have a narrow size distribution, and the average particle size is 0.191 μm. At a sintering temperature of 950 °C, a certain portion of the particles becomes even bigger (Fig. 4(e)) and thereby showing an average size of 0.285 μm and a wide size distribution (Fig. 5(e)). To further raise the sintering temperature to 1000 °C, all particles merge into large pieces (Fig. 4(f)) and start to densify (see the inset). It is clear that the average size D of NiCuZn ferrite particles increases with increasing sintering temperature, which is in accordance with the result of XRD analysis.

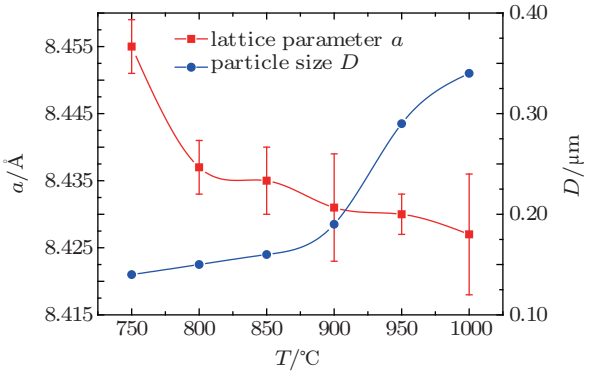


Fig. 3. (color online) Variations of lattice parameter a and particle size D (estimated by the Scherrer formula) with sintering temperature adopted for the generation of NiCuZn-ferrite powder samples.

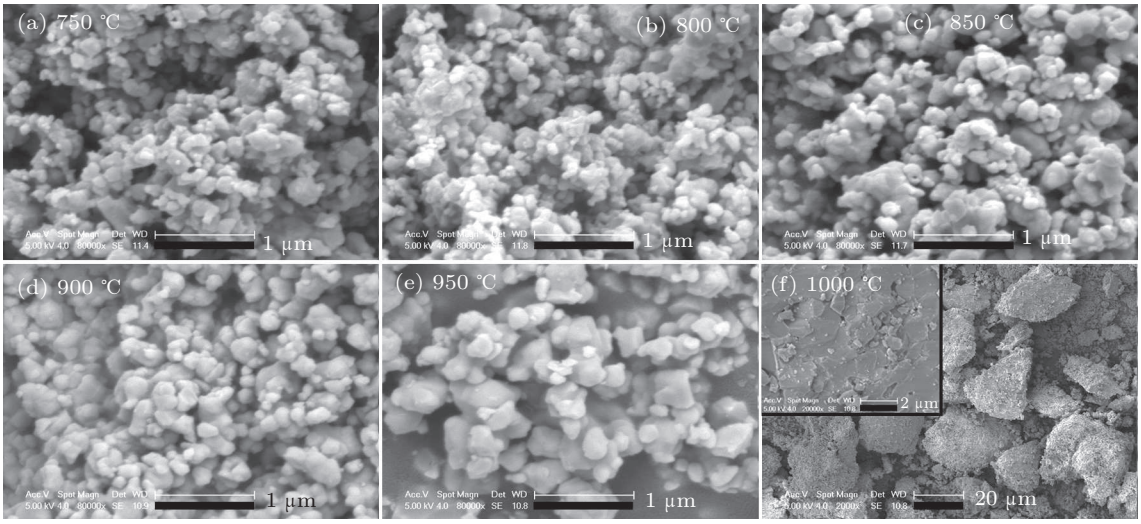


Fig. 4. SEM images of NiCuZn-ferrite powder samples generated after sintering at different temperatures for 3 h. Shown at the top left corner of (f) is the corresponding high-magnification SEM image.

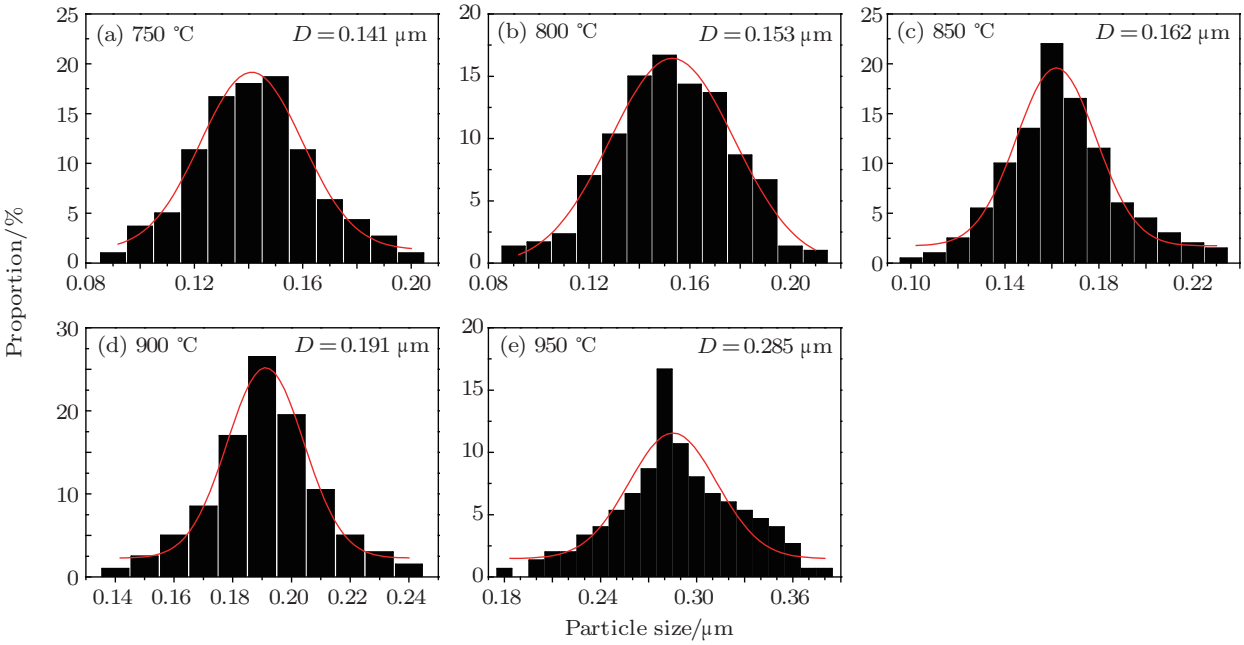


Fig. 5. (color online) Size distribution histograms (obtained by the Nano Measurer software based on the measured SEM images) of NiCuZn-ferrite powder samples generated after sintering at different temperatures for 3 h. The solid curves represent the results of Gaussian fitting. Shown at the top right corner is the corresponding average particle size D.

Indeed, in many studies,[3,20–23,38,39] a lot of methods of reducing sintering temperatures of high-permeability NiZn ferrites were considered. Hu *et al.*[3] indicated that optimum additions of CuO and V_2O_5 contributed to the grain growth and the densification of matrix in the sintering process, leading to decrease in sintering temperature of NiZn ferrite. Then they found that a NiZn ferrite with initial permeability as high as 1618 can be obtained at only 930 °C sintering temperature, using raw materials of 0.8-μm average particle size and adding 10-mol% CuO and 0.20-mol% V_2O_5. At the same time, Hsu *et al.*[38] found that Cu substitution for Ni in NiZn ferrite would enhance the densification of the ferrite, subsequently increase the μ value (initial permeability) and B_s value (saturation induction), and reduce the H_C value (coercivity) of the sintered ferrite. So they concluded that the NiCuZn ferrite powders with high Cu content could be sintered at about 800 °C, and the 900 °C-sintered sample has the perfect magnetic performance ($\mu_{f=1\ \mathrm{MHz}} = 390$, $H_C = 0.7$ Oe, $B_s \approx 3100$ Gs, 1 Gs = 10^{-4} T). Furthermore, Yan and Hu[39] have conducted a comparative research of the sintering process of NiCuZn ferrite. They found that microwave sintering technique can effectively promote the forward diffusion of ions and thus accelerate the sintering process, resulting in the grain growth and the densification of the matrix. Using microwave sintering technique, for the $Ni_{0.20}Zn_{0.60}Cu_{0.20}Fe_{1.98}O_4$ ferrite, the relative initial permeability μ_i of about 2000 was achieved at sintering tem-

perature of 980 °C. Actually, the effects of the additives and sintering process on magnetic performance are essentially due to the difference in microstructure between ferrite particles. Here, the results of XRD and SEM analyses appear to confirm this viewpoint. Therefore, it can be expected that the sintering temperature of 900 °C will be the best condition for the conventional sintering technique of NiCuZn ferrite. This will also be confirmed by the magnetic analysis in the following.

With such significant changes in structure, shape, average size, and size distribution, it is apparent that the heat treatment has great influence on grain growth. During low-temperature sintering (for example, 750 °C and 800 °C), there is structural transformation of ferrite particles, resulting in more internal defects and thereby suppressing the massive aggregation of interior crystal grains; then, also making the growth of particles imperceptible.[40] In fact, an appropriate sintering temperature (for example, 900 °C) is conducive to not only the full growth of crystals, but also the formation of grains with small size and narrow size distribution. If the temperature adopted for the sintering of NiCuZn-ferrite powder is too high (for example, 1000 °C), the melting zone between the micro-interfaces is enlarged, consequently resulting in the abnormal growth of particles and debasing its performance.

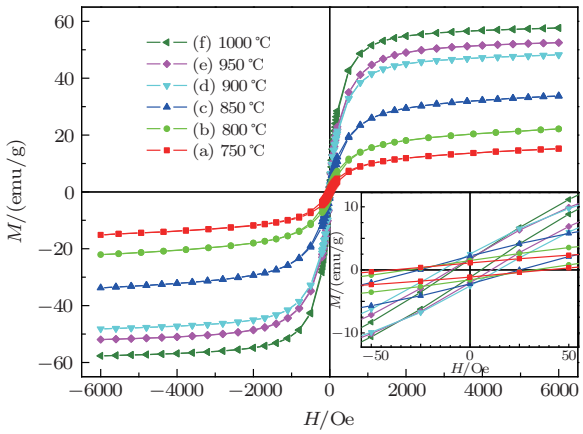


Fig. 6. (color online) Room-temperature hysteresis loops of NiCuZn-ferrite powder samples generated after sintering at different temperatures for 3 h. The inset shows the measurements around the origin.

We examine the magnetic properties of M1–M6 using VSM at room temperature. As shown in Fig. 6, all six samples show soft-magnetic behaviors (with small coercivity H_C and remanent magnetization M_r), and high values of saturation magnetization (M_s) at an applied field of 6 kOe. The most important magnetic parameters of NiCuZn ferrites, viz. M_s, M_r, and H_C are calculated as[41]

$$M_s = (|M_{s+}| + |M_{s-}|)/2, \quad M_r = (|M_{r+}| + |M_{r-}|)/2,$$
$$H_C = (|H_{C+}| + |H_{C-}|)/2, \tag{2}$$

where the subscript symbols '+' and '−' denote the positive and negative values of the above parameters, respectively, thus the H_C, M_r, and M_s values are listed in Table 1.

Figure 7 demonstrates how the magnetic properties change with sintering temperature. One can see that M_s increases and H_C decreases monotonically with the rise of sintering temperature. At the same time, M_r first increases and then decreases with increasing sintering temperature. As is well known, the saturation magnetization of a material is related to the crystallinity of the sample. With sintering temperature increasing, the density and the crystallinity are improved, thereby resulting in the increase of saturation magnetization.

In general, coercivity H_C can be expressed as the following two formulas:[41,42]

$$H_C \propto \frac{K_1 + 3\lambda_s\sigma/2}{\mu_0 M_s}, \tag{3}$$

$$H_C \propto \frac{\beta^{2/3}}{\mu_0 M_s}, \tag{4}$$

where K_1 denotes the contribution of magnetocrystalline anisotropy, λ_s is the saturated magnetostriction coefficient, σ denotes the internal stress, μ_0 is the space permeability, M_s is the saturation magnetization, and β denotes the volume concentration of impurities. From the above expressions it follows that H_C is closely related to the microstructure of ferrite magnetic material. For reducing coercivity to obtain better soft-magnetic properties, this can be accomplished by reducing the magnetocrystalline anisotropy, lowering the saturated magnetostriction coefficient, removing the internal stress, reducing the density of defects and the impurity content and increasing the saturation magnetization. Considering our samples, the significant increases of the average particle size D, compactness and crystallinity with the rise of sintering temperature, and the decreases of the impurity concentration, defect and stress, lead to the decrease of coercivity. In addition, it is considered that a decrease in lattice parameter a suggests the decline of crystalline anisotropy, and then leads to a reduction of H_C.

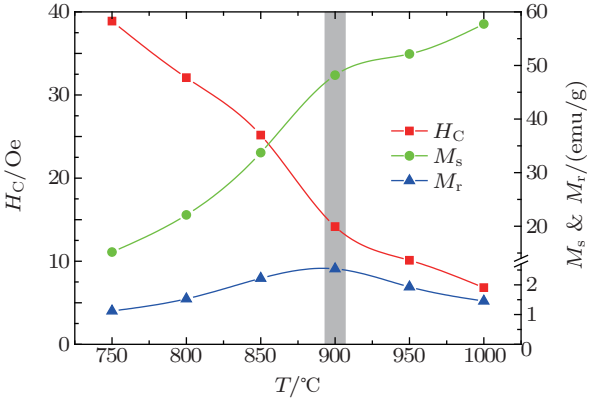


Fig. 7. (color online) Variations of coercivity H_C, saturation magnetization M_s, and remanent magnetization M_r with sintering temperature adopted for generating NiCuZn-ferrite powder samples.

Figures 1–7 reveal that CuO is a suitable additive to NiZn ferrites. As is well known, CuO can form a liquid phase at the initial stage of sintering and can be dissolved

in the matrix in the latter stage of sintering.[3,43] In addition, CuO can effectively reduce the synthesizing temperature of the spinel phase. Therefore, addition of CuO effectively promotes the solid reaction during sintering. Earlier studies have found that the solid reaction and densification process during sintering were restrained when CuO content was deficient.[3,38] As a result, the grain sizes were small, and pores appeared in the intergrain boundaries, while with increasing CuO content, the microstructures became more uniform and compact, and the intergranular pores disappeared and grains grew bigger. Obviously, such microstructures are favorable for improving the magnetic properties of ferrites. In the present work, we take advantage of an appropriate Cu content (i.e. $Ni_{0.276}Cu_{0.113}Zn_{0.604}Co_{0.008}Fe_{1.81}O_4$), yielding ideal microstructure and excellent performance.

In a word, there are several factors that assess the performance of NiCuZn-ferrite powder: good crystallinity, appropriate particle size, relatively low lattice parameter, uniform morphology, narrow size distribution, high compactness, etc. Based on this, the optimal sintering temperature is 900 °C, and the corresponding saturation magnetization and coercivity are about 48 emu/g and 14 Oe, respectively.

4. Conclusions

The solid-state reaction method is adopted to prepare high-performance NiCuZn-ferrite powders with pure spinel phase. In the process, commercial high-purity Fe_2O_3, NiO, and ZnO are used while CuO and Co_3O_4 serve as the additives. The influences of sintering temperature on crystal structure, particle size, morphology, and magnetic properties of NiCuZn ferrites are investigated. The results show that the optimal sintering temperature is 900 °C. The change of coercivity H_C can be attributed to the combined effects of particle size D, lattice parameter a, and the microstructure itself. The optimal submicron NiCuZn-ferrite powder is granular in shape and uniform in size ($D \approx 0.19$ μm), showing magnetic parameters of $H_C = 14$ Oe and $M_s = 48$ emu/g. The adopted process is convenient, economical, and reproducible for generating the ferrite powder which is suitable for manufacturing the high-permeability product.

References

[1] Cullity B D and Graham C D 2009 *Introduction to Magnetic Materials*, 2nd edn (Piscataway, NJ: IEEE)

[2] Dimri M C, Verma A, Kashyap S C, Dube D C, Thakur O P and Prakash C 2006 *Mater. Sci. Eng. B* **133** 42

[3] Hu J, Yan M and Luo W 2005 *Physica B* **368** 251

[4] Tsay C Y, Liu K S, Lin T F and Lin I N 2000 *J. Magn. Magn. Mater.* **209** 189

[5] Lima U R, Nasar M C, Nasar R S, Rezende M C, Araújo J H and Oliveira J F 2008 *Mater. Sci. Eng. B* **151** 238

[6] Sakellari D, Tsakaloudi V, Polychroniadis E K and Zaspalis V 2008 *J. Am. Ceram. Soc.* **91** 366

[7] Su H, Zhang H W, Tang X L, Zhong Z Y and Jing Y L 2009 *Mater. Sci. Eng. B* **162** 22

[8] Reddy N R, Ramana M V, Rajitha G, Rajagopal E, Sivakumar K V and Murthy V R K 2005 *J. Magn. Magn. Mater.* **292** 159

[9] Aphesteguy J C, Damiani A, DiGiovanni D and Jacobo S E 2009 *Physica B* **404** 2713

[10] Tong S Y, Tung M J, Ko W S, Huang Y T, Wang Y P, Wang L C and Wu J M 2013 *J. Alloys Compd.* **550** 39

[11] Sun K, Lan Z W, Yu Z, Jiang X N and Huang J M 2011 *J. Magn. Magn. Mater.* **323** 927

[12] Roy P K and Bera J 2008 *J. Mater. Process. Technol.* **197** 279

[13] Su H, Zhang H W, Tang X L and Liu Y L 2007 *J. Mater. Sci.* **42** 2849

[14] Sorescu M, Diamandescu L, Peelamedu R, Roy R and Yadoji P 2004 *J. Magn. Magn. Mater.* **279** 195

[15] Barba A, Clausell C, Feliu C and Monzo M 2004 *J. Am. Ceram. Soc.* **87** 571

[16] Makovec D, Drofenik M and Znidarsic A 1999 *J. Am. Ceram. Soc.* **82** 1113

[17] Caltun O F, Spinu L and Stancu A 2001 *IEEE Trans. Magn.* **37** 2353

[18] Morrison S A, Cahill C L, Carpenter E E, Calvin S, Swaminathan R, McHenry M E and Harris V G 2004 *J. Appl. Phys.* **95** 6392

[19] Harris V G, Fatemi D J, Cross J O, Carpenter E E, Browning V M, Kirkland J P, Mohan A and Long G J 2003 *J. Appl. Phys.* **94** 496

[20] Dimri M C, Kashyap S C and Dube D C 2010 *Phys. Status Solidi A* **207** 396

[21] Ghasemi A, Ghasemi E and Paimozd E 2011 *J. Magn. Magn. Mater.* **323** 1541

[22] Su H, Tang X L, Zhang H W, Jing Y L and Zhong Z Y 2011 *J. Magn. Magn. Mater.* **323** 592

[23] Su H, Zhang H W, Tang X L, Liu B Y and Zhong Z Y 2009 *J. Alloys Compd.* **475** 683

[24] Reddy M P, Balakrishnaiah G, Madhuri W, Ramana M V, Reddy N R, Kumar K V S, Murthy V R K and Reddy R R 2010 *J. Phys. Chem. Solids* **71** 1373

[25] Yang Q H, Zhang H W, Liu Y L, Wen Q Y and Jia L J 2012 *Mater. Lett.* **79** 103

[26] Lee Y H, Kuan W C and Tuan W H 2013 *J. Eur. Ceram. Soc.* **33** 95

[27] Jadhav P A, Devan R S, Kolekar Y D and Chougule B K 2009 *J. Phys. Chem. Solids* **70** 396

[28] Byun T Y, Byeon S C, Hong K S and Kim C K 1999 *IEEE Trans. Magn.* **35** 3445

[29] Sugimoto M 1999 *J. Am. Ceram. Soc.* **82** 269

[30] Smit J and Wijn H P J 1955 *Ferrites* (Eindhoven: Philips Technical Library)

[31] Dimri M C, Kashyap S C, Dube D C and Mohanta S K 2006 *J. Electroceram.* **16** 331

[32] Hsiang H I, Cheng P W and Yen F S 2012 *Ceram. Int.* **38** 4915

[33] Akther Hossain A K M, Seki M, Kawai T and Tabata H 2004 *J. Appl. Phys.* **96** 1273

[34] Dai J F, Jiang Y, Wang Q, Li W X and Dai Y L 2014 *Micro Nano Lett.* **9** 31

[35] Xiang J, Shen X Q, Song F Z and Liu M Q 2010 *J. Solid State Chem.* **183** 1239

[36] Klug H P and Alexander L E 1974 *X-Ray Diffraction Procedures*, 2nd edn. (New York: Wiley-Interscience)

[37] Cowley J M 1981 *Diffraction Physics*, 2nd edn. (Amsterdam: North-Holland)

[38] Hsu W C, Chen S C, Kuo P C, Lie C T and Tsai W S 2004 *Mater. Sci. Eng. B* **111** 142

[39] Yan M and Hu J 2006 *J. Magn. Magn. Mater.* **305** 171

[40] Li Y H, Kim W and Kim C S 2011 *J. Appl. Phys.* **109** 07A505

[41] Kojima H 1982 *Ferromagnetic Materials*, Vol. 3, ed. Wohlfarth E P (Amsterdam: North-Holland)

[42] Morrish A H 2001 *The Physical Principles of Magnetism* (Piscataway, NJ: IEEE)

[43] Ahmed T T, Rahman I Z and Rahman M A 2004 *J. Mater. Process. Technol.* **153–154** 797